International Journal of
Mathematical Modelling & Computations
Vol. 07, No. 01, Winter 2017, 39- 54

The Comparison of Two High-Order Semi-Discrete Central Schemes for Solving Hyperbolic Conservation Laws

R. Abedian [a,*]
[a] *University of Tehran, Faculty of Engineering, Department of Engineering Science, P.O. 14395-195,Tehran, Iran.*

Abstract. This work presents two high-order, semi-discrete, central-upwind schemes for computing approximate solutions of 1D systems of conservation laws. We propose a central weighted essentially non-oscillatory (CWENO) reconstruction, also we apply a fourth-order reconstruction proposed by Peer et al., and afterwards, we combine these reconstructions with a semi-discrete central-upwind numerical flux and the third-order TVD Runge-Kutta method. Also this paper compares the numerical results of these two methods. Afterwards, we are interested in the behavior of the total variation (TV) of the approximate solution obtained with these schemes. We test these schemes on both scalar and gas dynamics problems. Numerical results confirm that the new schemes are non-oscillatory and yield sharp results when solving profiles with discontinuities. We also observe that the total variation of computed solutions is close to the total variation of the exact solution or a reference solution.

Received: 11 October 2016, Revised: 22 January 2013, Accepted: 28 February 2013.

Keywords: CWENO technique, Central-Upwind schemes, Hyperbolic conservation laws, Total variation.

Index to information contained in this paper

1. Introduction

Hyperbolic systems of conservation laws

$$u_t + f(u)_x = 0 \qquad u \in \mathbb{R}^d, \ d \geqslant 1, \tag{1}$$

arise in many practical problems such as Biological models [25], shallow water flow [23], Discrete kinetic models [5], and many other areas in science and engineering.

*Corresponding author. Email: rabedian@ut.ac.ir.

Analytical solutions are available only in very few special cases. Therefore, the numerical solution of hyperbolic systems of conservation laws has been an important field of research for the last decades.

The schemes more commonly used in context are the so-called shock capturing schemes(see for example the book by LeVeque [15]). Among shock capturing schemes, the most commonly used are finite volume schemes. For these schemes, the conservation laws are integrated in space and time on control volumes. Therefore the equation is transformed in integral form. In this formulation, to update the solution and the cell averages, it is necessary to evaluate numerical intermediate values of the quadrature formula and flux functions at the edge of each cell.Among finite volume methods, one should distinguish between *upwind* and *central* schemes.

The prototype of upwind schemes is first order upwind, which is first order Godunov method [6], based on the solution of the Riemann problem at cell edges. The prototype of central schemes is first order Lax-Friedrichs (LxF) scheme [4]. Like the Godunov method, it is based on piecewise constant approximate solution and unlike the Godunov method, the LxF scheme is Riemann-solver-free.

Generally, upwind schemes gain sharper resolution than central schemes for the same order of accuracy and spatial grids because they require some knowledge about the eigenstructure , but are more expensive, and are more complicated to be implemented. For this reason, in recent years, central schemes got considerable attention.

This work has focused on the class of central schemes i.e. schemes that can be implemented with very little knowledge of the structure of the system of conservation laws. Since the central schemes are Riemann-solver-free, these schemes are simple to be implemented, and can be extended to multi-dimensional problems.

Central-upwind schemes are semi-discrete variants of central schemes which have improved efficiency and less dissipation than fully-discrete central schemes. A second-order semi-discrete central scheme was introduced by Kurganov and Tadmor in [13]. The basic idea in the construction of the second-order semi-discrete scheme was to use more accurate information about the local speed of propagation of the discontinuities. Modifications to this scheme, based on the one-sided local speed of propagation, were proposed by Kurganov, Noelle and Petrova in [11]. These schemes for the evolution step employ integration over Riemann fans and do not require a Riemann solver and characteristic decomposition, so they are Godunov-type central schemes. Also, they have an upwind nature, since one-sided information is used to estimate the width of the Riemann fans.

In this work, we propose a high-order CWENO reconstruction, also we apply fourth-order reconstruction proposed in [21]. The new schemes use the numerical flux of [11], refered to as the KNP flux. We combine the KNP flux with these reconstructions, and the third-order TVD Runge-Kutta scheme, proposed in [24].

Also in this work, we investigate the question of the convergence of the semi-discrete central scheme for approximating solutions of hyperbolic systems of conservation laws. We numerically test the behavior of the total variation (TV), $TV(u) := \sum_j |u_{j+1} - u_j|$, of the discrete solution. In the case of systems, TV is defined as the sum of the TV over the components.

A scheme is called total variation bounded (TVB) in $0 \leqslant t \leqslant T$, if $TV(u^n) \leqslant K$ for fixed positive K (constant K depends only on the initial condition), and $\forall n,\ \Delta t\ s.t.\ n\Delta t \leqslant T$. If $TV(u^{n+1}) \leqslant TV(u^n)$ then the scheme is total variation diminishing (TVD). If a scheme is TVB, then there exists a convergent subsequence in L^1_{LOC} to a weak solution of (1), which turns into strong convergence if an additional entropy condition is satisfied (see [15] for more details). Our numerical results suggest that our schemes are TVB which provides evidence of the

convergence of the scheme.

The structure of this paper is as follows: In Section 2 we present our high-order central-upwind schemes. For do that, we give a brief overview of the derivation of the KNP flux in Section 2.1. The CWENO reconstruction is summarized in Section 2.2. Also, the fourth-order reconstruction proposed in [21] is summarized in Section 2.3. Next, in Section 3 we present the results of a number of numerical tests of our schemes. We test both the accuracy and the evolution of the total variation of the resulting approximations. Finally, Section 4 ends this paper with a brief summary.

2. Semi-Discrete Central-Upwind

In this Section we give a brief overview of the components which we use to construct our central-upwind schemes. The problem is required to be hyperbolic, i.e. the flux Jacobian

$$\mathbf{A} = \frac{\partial f(u)}{\partial u} \tag{2}$$

is required to have both real eigenvalues $\lambda_1 \leqslant \lambda_2 \leqslant \cdots \leqslant \lambda_N$ and a complete set of eigenvectors. If the real eigenvalues are distinct then the problem is strictly hyperbolic and a complete set of eigenvectors is guaranteed.

2.1 *The KNP Flux*

Consider a uniform spatial grid where the cell $I_j = [x_{j-}, x_{j+}]$ has a width h. Let the approximation to the cell average of u on I_j be given by $\bar{u}_j^n = \frac{1}{h}\int_{I_j} u(x,t^n)dx$. We assume that the cell averages $\{\bar{u}_j^n\}$ are known at time t^n. Let $\chi_j(x)$ be the characteristic function of the cell I_j. First, from $\{\bar{u}_j^n\}$, a piecewise polynomial $\tilde{u}(x,t^n) := \sum_j P_j(x)\chi_j(x)$ was reconstructed. Here, $P_j(x)$ are polynomials of a suitable degree.The point-values of $\tilde{u}(x,t^n)$ at the interfaces of the cell I_j are denoted by $u_{j+}^+ := P_{j+1}(x_{j+})$ and $u_{j+}^- := P_j(x_{j+})$. The left- and right-sided local speeds of propagation of information from the discontinuities at the cell interfaces, a_{j+}^1, a_{j+}^N, are estimated by

$$a_{j+}^N = \max\left[\lambda_N\left(\frac{\partial f}{\partial u}(u_{j+}^-)\right), \lambda_N\left(\frac{\partial f}{\partial u}(u_{j+}^+)\right), 0\right], \tag{3}$$

and

$$a_{j+}^1 = \min\left[\lambda_1\left(\frac{\partial f}{\partial u}(u_{j+}^-)\right), \lambda_1\left(\frac{\partial f}{\partial u}(u_{j+}^+)\right), 0\right]. \tag{4}$$

These local speeds of propagation are used to determine intervals for averaging that contain the Riemann fans from the cell interfaces. For more details see [11].

One-dimensional grid updates of the average conserved variables are calculated using a conservative update as

$$\frac{d}{dt}\bar{u}_j(t) = -\frac{H_{j+} - H_{j-}}{h}, \tag{5}$$

the numerical flux(KNP) in (5) is given by

$$H_{j+} = \frac{a^N_{j+} f(u^-_{j+}) - a^1_{j+} f(u^+_{j+})}{a^N_{j+} - a^1_{j+}} + \frac{a^N_{j+} a^1_{j+}}{a^N_{j+} - a^1_{j+}} (u^+_{j+} - u^-_{j+}). \tag{6}$$

The accuracy of this scheme is determined by the accuracy of the reconstructions and the ODE solver.

2.2 *The CWENO Reconstruction*

In the framework of upwind schemes, high-order essentially non-oscillatory(ENO) reconstructions were proposed in [7]. ENO schemes choose the stencil that provide the least oscillatory reconstruction. Weighted essentially non-oscillatory (WENO) reconstructions were described by Liu et al. in [19]. Later, Jiang and Shu in [9] described improved smoothness indicators and efficient implementations of WENO schemes. In [3] high-order ENO reconstructions were first combined with central schemes. A central WENO(CWENO) reconstruction for 1D hyperbolic conservation laws was proposed by Levy et al. in [16].

To derive an essentially non-oscillatory reconstruction, three supplementary polynomials ($P_L(x), P_R(x)$ and $P_C(x)$), approximating $u(x)$ with a lower accuracy on I_j, are needed to define. Thus, the polynomial of second-order accuracy, $P_L(x)$, is defined on the reduced stencil $\{I_{j-2}, I_{j-1}, I_j\}$, $P_C(x)$ is defined on the stencil $\{I_{j-1}, I_j, I_{j+1}\}$, whereas $P_R(x)$ is defined on the stencil $\{I_j, I_{j+1}, I_{j+2}\}$. Each of these polynomials is constructed by posing the following interpolation requirements:

$$\int_{x_{j+l-}}^{x_{j+l+}} P_L(x)dx = h\bar{u}^n_{j+l}, \qquad l = -2, -1, 0,$$

$$\int_{x_{j+l-}}^{x_{j+l+}} P_C(x)dx = h\bar{u}^n_{j+l}, \qquad l = -1, 0, 1,$$

$$\int_{x_{j+l-}}^{x_{j+l+}} P_R(x)dx = h\bar{u}^n_{j+l}, \qquad l = 0, 1, 2.$$

Since $\deg(P_k(x))=2$, $k = L, C, R$, one can rewrite

$$P_k(x) = \sum_{j=0}^{2} \frac{a_j}{j!} (\frac{x - x_j}{h})^j, \qquad k = L, C, R.$$

For $P_L(x)$ defined on $\{I_{j-2}, I_{j-1}, I_j\}$ and $P_R(x)$ defined on $\{I_j, I_{j+1}, I_{j+2}\}$, the coefficients are respectively(left to right),

$$\begin{cases} a_0 = \frac{23}{24}\bar{u}^n_j + \frac{1}{12}(\bar{u}^n_{j-1} - \bar{u}^n_{j-2}), \\ a_1 = \bar{u}^n_{j-2} - 2\bar{u}^n_{j-1} + \frac{3}{2}\bar{u}^n_j, \\ a_2 = \bar{u}^n_{j-2} - 2\bar{u}^n_{j-1} + \bar{u}^n_j, \end{cases} \qquad \begin{cases} a_0 = \frac{23}{24}\bar{u}^n_j + \frac{1}{12}(\bar{u}^n_{j+1} - \bar{u}^n_{j+2}), \\ a_1 = -\bar{u}^n_{j+2} + 2\bar{u}^n_{j+1} - \frac{3}{2}\bar{u}^n_j, \\ a_2 = \bar{u}^n_{j+2} - 2\bar{u}^n_{j+1} + \bar{u}^n_j. \end{cases}$$

And for $P_C(x)$ defined on $\{I_{j-1}, I_j, I_{j+1}\}$

$$\begin{cases} a_0 = \frac{13}{12}\bar{u}_j^n - \frac{1}{24}(\bar{u}_{j+1}^n + \bar{u}_{j-1}^n), \\ \\ a_1 = (\bar{u}_{j+1}^n - \bar{u}_{j-1}^n), \\ \\ a_2 = \bar{u}_{j+1}^n - 2\bar{u}_j^n + \bar{u}_{j-1}^n. \end{cases}$$

The reconstruction is created by considering a convex combination of the above polynomials,

$$P_j(x) = w_L P_L(x) + w_C P_C(x) + w_R P_R(x),$$
$$w_i \geqslant 0 \ \ \forall i \in \{L, C, R\}, \qquad \sum_i w_i = 1. \quad (7)$$

As already noted in [18], in smooth regions, the coefficients w_i of the convex combination in (7) are chosen to guarantee the maximum order of accuracy (in this particular case, order three), but in the presence of a discontinuity they are automatically switched to the best one-sided stencil (which generates the least oscillatory reconstruction). Following the notations of [24], the weights, w_i, are written as

$$w_i = \frac{\alpha_i}{\sum_m \alpha_m}, \qquad \alpha_i = \frac{C_i}{(\epsilon + IS_i)^2}, \qquad i, m \in \{L, C, R\}.$$

The constant ϵ guarantees that the denominator does not vanish and is empirically taken as $\epsilon = 10^{-6}$. Also, the smoothness indicators, IS_i, are defined as

$$IS_i = \sum_{l=1}^{2} \int_{x_{j-}}^{x_{j+}} h^{2l-1} (P_i^{(l)}(x))^2 dx.$$

An explicit integration then results in

$$IS_i = a_1^2 + \frac{13}{12} a_2^2, \qquad i \in \{L, C, R\}.$$

As already noted in [18], the freedom in selecting these constants, C_i, has no influence on the properties of the numerical stencil; any symmetric choice, provides the desired accuracy for $P_j(x)$.

Remark. In the above equations in order to simplify the notations, the upper index j has been omited. We should remember that the weights and the three polynomials change from cell to cell.

2.3 *The Fourth-Order Reconstruction of Peer et al.*

This subsection gives a brief review of reconstruction, for further details see [21]. Polynomial $P_j(x)$ is considered on I_j in the form:

$$P_j(x) = u_j^n + u_j'(\frac{x - x_j}{h}) + \frac{1}{2!} u_j''(\frac{x - x_j}{h})^2 + \frac{1}{3!} u_j'''(\frac{x - x_j}{h})^3, \quad x \in I_j.$$

Here, $u_j^n, u_j'/h, u_j''/h^2$, and u_j'''/h^3 are the approximate point values and the first, second, and third derivatives of $u(x,t^n)$ at $x = x_j$, which are reconstructed from the cell averages, $\{\bar{u}_j^n\}$. It should be noted that this reconstruction [21] satisfies the following three properties:

- $\mathcal{P}1-$ conservation of cell averages: $\bar{P}_j(x)|_{x=x_j} = \bar{u}_j^n$.
- $\mathcal{P}2-$ Accuracy: $\tilde{u}(x,t^n) = u(x,t^n) + \mathcal{O}(h^4)$.
- $\mathcal{P}3-$ Non-oscillatory behavior of $\sum_j P_j(x)\chi_j(x)$.

Here $\bar{P}_j(x) = \frac{1}{h}\int_{I_j} P_j(x)dx$, and $\chi_j(x)$ is the characteristic function of I_j.

In order to guarantee property $\mathcal{P}1$, u_j^n must satisfy

$$u_j^n = \bar{u}_j^n - \frac{u_j''}{24}. \tag{8}$$

Remark : Starting with third-order and higher-order accurate methods, the point values aren't equal with cell averages, $u_j^n \neq \bar{u}_j^n$.

The NT scheme [20] uses a second-order accurate limiter for the numerical derivative u_j' in the form

$$u_j' = \mathbf{MM}(\Delta\bar{u}^n_{j-\frac{1}{2}}, \Delta\bar{u}^n_{j+\frac{1}{2}}). \tag{9}$$

Here, $\Delta\bar{u}^n_{j+\frac{1}{2}} = \bar{u}^n_{j+1} - \bar{u}^n_j$ and the MinMod limiter (**MM**) is defined by

$$\mathbf{MM}(x_1, x_2, \cdots) = \begin{cases} \min_p\{x_p\} \text{ if } x_p > 0 \ \ \forall p, \\ \max_p\{x_p\} \text{ if } x_p < 0 \ \ \forall p, \\ 0 \qquad \text{otherwise.} \end{cases}$$

The accuracy of (9) decreases when $\Delta\bar{u}_{j-\frac{1}{2}}\Delta\bar{u}_{j+\frac{1}{2}} < 0 = u_j'$. Thus, the NT scheme modified the uniform non-oscillatory (UNO) limiter of Harten and Osher [8] by adding second-order differences to (9) to get high accuracy,

$$u_j' = \mathbf{MM}\Big(\Delta\bar{u}^n_{j-\frac{1}{2}} + \frac{1}{2}\mathbf{MM}(\Delta^2\bar{u}^n_{j-1}, \Delta^2\bar{u}^n_j), \\ \Delta\bar{u}^n_{j+\frac{1}{2}} - \frac{1}{2}\mathbf{MM}(\Delta^2\bar{u}^n_j, \Delta^2\bar{u}^n_{j+1})\Big), \tag{10}$$

where $\Delta^2\bar{u}_j^n = \Delta\bar{u}^n_{j+\frac{1}{2}} - \Delta\bar{u}^n_{j-\frac{1}{2}}$.

In order to satisfy properties $\mathcal{P}2-\mathcal{P}3$ the modified UNO limiter of [22] has been used. Similar to the numerical derivative (9), u_j''' depends on its two neighboring third-order differences

$$u_j''' = \mathbf{MM}(\Delta^3\bar{u}^n_{j-\frac{1}{2}}, \Delta^3\bar{u}^n_{j+\frac{1}{2}}), \tag{11}$$

where $\Delta^3\bar{u}^n_{j+\frac{1}{2}} = \Delta^2\bar{u}^n_{j+1} - \Delta^2\bar{u}^n_j$. For obtaining fourth-order accurate approxima-

tions of the first derivative, put

$$u'_j = \mathbf{MM}\Big(\Delta\bar{u}^n_{j-\frac{1}{2}} + \frac{1}{2}\mathbf{MM}(\Delta^2\bar{u}^n_{j-1} + \frac{7}{12}u'''_{j-1}, \Delta^2\bar{u}^n_j - \frac{5}{12}u'''_j), \\ \Delta\bar{u}^n_{j+\frac{1}{2}} - \frac{1}{2}\mathbf{MM}(\Delta^2\bar{u}^n_j + \frac{5}{12}u'''_j, \Delta^2\bar{u}^n_{j+1} - \frac{7}{12}u'''_{j+1})\Big). \quad (12)$$

Remark: From (12), there are eight candidates for u'_j as following:
- $\Delta\bar{u}_{j-} + (\Delta^2\bar{u}_{j-1} + \frac{7}{12}\Delta^3\bar{u}_{j-\frac{3}{2}})$,
- $\Delta\bar{u}_{j-} + (\Delta^2\bar{u}_{j-1} + \frac{7}{12}\Delta^3\bar{u}_{j-})$,
- $\Delta\bar{u}_{j-} + (\Delta^2\bar{u}_{j} - \frac{5}{12}\Delta^3\bar{u}_{j-})$,
- $\Delta\bar{u}_{j-} + (\Delta^2\bar{u}_{j} - \frac{5}{12}\Delta^3\bar{u}_{j+})$,
- $\Delta\bar{u}_{j+} - (\Delta^2\bar{u}_{j} + \frac{5}{12}\Delta^3\bar{u}_{j-})$,
- $\Delta\bar{u}_{j+} - (\Delta^2\bar{u}_{j} + \frac{5}{12}\Delta^3\bar{u}_{j+})$,
- $\Delta\bar{u}_{j+} - (\Delta^2\bar{u}_{j+1} - \frac{7}{12}\Delta^3\bar{u}_{j+})$,
- $\Delta\bar{u}_{j+} - (\Delta^2\bar{u}_{j+1} - \frac{7}{12}\Delta^3\bar{u}_{j+\frac{3}{2}})$.

Now, by considering the Taylor series expansion of function $u(x)$ around the point x_j and definition of $\bar{u}_j = \frac{1}{h}\int_{I_j} u(x)dx$, we obtain

$$\Delta\bar{u}_{j-} + (\Delta^2\bar{u}_{j-1} + \frac{7}{12}\Delta^3\bar{u}_{j-\frac{3}{2}}) \\ = (-7/24)\bar{u}_{j-3} + (33/24)\bar{u}_{j-2} + (-69/24)\bar{u}_{j-1} + (43/24)\bar{u}_j = u'_j + \mathcal{O}(h^4).$$

Similarly, for seven other candidates, we have the above result, then the formula in (12) is a consistent approximation of $u'(x_j)$.

Also, in order to approximate the point values u^n_j of (8) from the cell averages $\{\bar{u}^n_j\}$, we put

$$u''_j = \mathbf{MM}\Big(\Delta^2\bar{u}^n_{j-1} + u'''_{j-1}, \Delta^2\bar{u}^n_j, \Delta^2\bar{u}^n_{j+1} - u'''_{j+1}\Big). \quad (13)$$

3. Numerical Results

This section describes the results of numerical example on various test problem. The new semi-discrete CWENO reconstruction and reconstruction of Peer et al. schemes are abbreviated by SDCS (Semi Discrete Central Scheme) and SDPS (Semi Discrete Peer Scheme), respectively. The accuracy of the schemes are tested on problems with smooth solutions and solved various equations which admit non-smooth solutions. Also the total variation(TV) of the numerical experiments are tested. To integrate (5) forward in time, the third-order TVD Runge-Kutta method is used. We also ran our examples with the standard Runge-Kutta method and observed no significant change in the results. In all the numerical experiments below, the CFL number is equal to $0.45\min_j \frac{h}{|\lambda_j|}$, where here λ_j denote the eigenvalues of the Jacobian of f evaluated at x_j.

Remark : It should be noted that in Figures, results obtained using the methods of SDPS, SDCS and exact or reference solution are shown by " $\times$ ", " . " and solid line respectively.

Table 1. Errors and orders of convergence for advection equation at T=2.

N	L_1 error	L_1 order	L_∞ error	L_∞ order
SDPS scheme				
25	0.1256(-2)	-	0.1859(-2)	-
50	0.9272(-4)	3.7598	0.2098(-3)	3.1474
100	0.6477(-5)	3.8395	0.2191(-4)	3.2594
200	0.4535(-6)	3.8362	0.2452(-5)	3.1596
400	0.2324(-7)	4.2864	0.2736(-6)	3.1638
SDCS scheme				
25	0.8267(-3)	-	0.5437(-3)	-
50	0.6838(-4)	3.5957	0.5223(-4)	3.3799
100	0.8289(-5)	3.0443	0.6482(-5)	3.0104
200	0.1040(-5)	2.9946	0.7159(-6)	3.1786
400	0.1295(-6)	3.0056	0.8017(-7)	3.1586

Table 2. Errors and orders of convergence for Test 1 with different ideal weights (SDCS scheme with different constants)

N	L_1 error	L_1 order	L_∞ error	L_∞ order
$C_L = C_R = \frac{1}{4}, C_C = \frac{3}{4}$				
25	0.1259(-2)	-	0.1855(-2)	-
50	0.9270(-4)	3.7636	0.2094(-3)	3.1471
100	0.6476(-5)	3.8394	0.2197(-4)	3.2527
200	0.4538(-6)	3.8350	0.2450(-5)	3.1647
400	0.2322(-7)	4.2886	0.2734(-6)	3.1637
$C_L = C_R = \frac{1}{16}, C_C = \frac{7}{8}$				
25	0.1260(-2)	-	0.1794(-2)	-
50	0.9201(-4)	3.7755	0.2083(-3)	3.1064
100	0.6471(-5)	3.8297	0.2192(-4)	3.2483
200	0.4524(-6)	3.8383	0.2441(-5)	3.1667
400	0.2324(-7)	4.2829	0.2727(-6)	3.1621
$C_L = \frac{2}{4}, C_R = \frac{1}{4}, C_C = \frac{1}{4}$				
25	0.9231(-3)	-	0.9754(-3)	-
50	0.4357(-3)	1.0832	0.7612(-3)	0.3577
100	0.1789(-3)	1.2842	0.5639(-3)	0.4328
200	0.9870(-4)	0.8580	0.3459(-3)	0.7051
400	0.8231(-4)	0.2620	0.1229(-3)	1.4929

3.1 *Scalar Test Problems*

As first example, please consider the scalar linear hyperbolic equation

$$u_t + u_x = 0, \qquad x \in [-1, 1],$$

augmented with the smooth initial data, $u(x, 0) = \sin(\pi x)$, and periodic boundary conditions. This test is used to check the convergence rate. The L_1- and $L_\infty-$ norms of the errors and orders are shown in Table 1. The two schemes converge to third accuracy in L_∞, but SDPS converges to fourth accuracy in L_1 as the computational grid is refined. The L_1 and L_∞ errors and orders of convergence by SDCS with different weights are shwon in Table 2. As we expect, any symmetric choice of constants C_i provides the desired accuracy. Note that the TV of the exact solution equals 4, and remains constant along the evolution.

Next, we solve the linear advection equation $u_t + u_x = 0$, over the long time interval $T = 8$, on the same domain with periodic boundary conditions and initial condition $u_0(x)$ defined in the Example 1 of [9] as:

$$u(x,0) = \begin{cases} \frac{1}{6}(G(x, z-\delta) + G(x, z+\delta) + 4G(x, z)), & -0.8 \leqslant x \leqslant -0.6, \\ 1, & -0.4 \leqslant x \leqslant -0.2, \\ 1 - |10(x - 0.1)|, & 0 \leqslant x \leqslant 0.2, \\ \frac{1}{6}(F(x, a-\delta) + F(x, a+\delta) + 4F(x, a)), & 0.4 \leqslant x \leqslant 0.6, \\ 0, & \text{otherwise}, \end{cases}$$

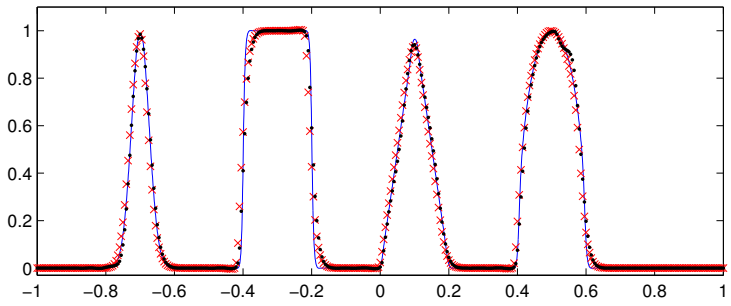

(a)

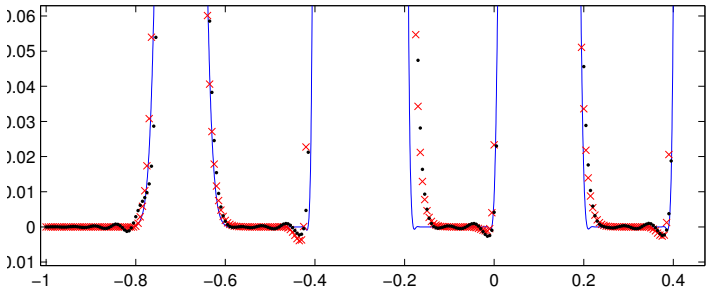

(b)

Figure 1. Test 2 by N=400 at T=8. (a): advection equation, and (b): zoomed region foot. SDPS, SDCS and exact solution are shown by " × ", " . " and solid line respectively.

where

$$G(x,z) = e^{-\beta(x-z)^2},$$

$$F(x,a) = (\max(1-\alpha^2(x-a)^2, 0))^{1/2}.$$

The constants are taken as $a = 0.5, z = -0.7, \delta = 0.005, \alpha = 10$, and $\beta = (\log 2)/36\delta^2$. Note that, this test is used to show the resolution properties of the schemes. Fig.1 displays the different approximation on 400 cells. SDPS gives an overall better approximation than SDCS. Also, the SDCS scheme generates oscillations at the foot of the waves. The approximations at $T = 8$ on 800 cells are illustrated in Fig. 2. As it can be seen, the SDPS scheme gives an overall better approximation than the SDCS scheme and is sharper at the top of the wave.

For the third test problem, the initial boundary value problem (IBVP) for the inviscid Burgers' equation

$$u_t + (\frac{u^2}{2})_x = 0, \qquad u(x,0) = 1 + 0.5\sin(\pi x), \qquad x \in [-1,1],$$

with periodic boundary conditions is considered. It is known that the unique entropy solution of the problem develops a shock discontinuity at $T_s = 2/\pi \simeq 0.7$. Accuracy of the schemes at T=0.12(before shock formation) is tested and the results are shown in Table 3. Also Table 4 presents the errors by SDPS and SDCS after the shock($T = 1.5$). Comparing the magnitude of errors by SDPS and SDCS

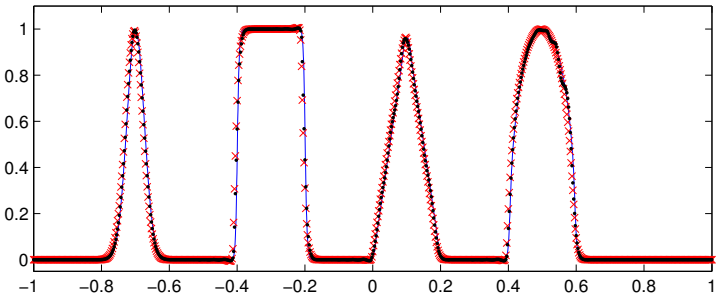

(a)

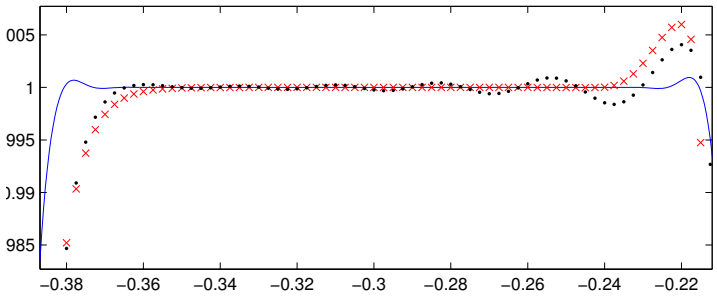

(b)

Figure 2. Test 2 by N=800 at T=8. (a): advection equation, and (b): zoomed region-wave top. SDPS, SDCS and exact solution are shown by " × ", " . " and solid line respectively.

Table 3. Errors and orders of convergence for Burgers' problem 3 at T=0.12.

N	L_1 error	L_1 order	L_∞ error	L_∞ order
SDPS scheme				
25	0.8041(-3)	-	0.4956(-3)	-
50	0.5081(-4)	3.9842	0.5334(-4)	3.2159
100	0.3282(-5)	3.9525	0.4817(-5)	3.4690
200	0.2349(-6)	3.8045	0.5508(-6)	3.1285
SDCS scheme				
25	0.9729(-3)	-	0.2500(-3)	-
50	0.7708(-4)	3.6579	0.1918(-4)	3.7043
100	0.7824(-5)	3.3004	0.1937(-5)	3.3077
200	0.9090(-6)	3.1056	0.2257(-6)	3.1013

Table 4. Errors for approximation of Test 3 at T=1.5.

	SDPS scheme		SDCS scheme	
N	L_1 error	L_∞ error	L_1 error	L_∞ error
25	0.3525(-1)	0.3071(0)	0.2975(-1)	0.2724(0)
50	0.1648(-1)	0.1934(0)	0.1374(-1)	0.1619(0)
100	0.2223(-2)	0.5182(-1)	0.2322(-2)	0.5402(-1)
200	0.1041(-2)	0.5008(-1)	0.9515(-3)	0.4487(-1)

schemes for this test problem shows that the SDCS yields better accuracy in both L_1 and L_∞ norms when $T = 1.5$.

Fig.3 shows the solution after shock formation at $T = 1.5$, and the change in the TV of the approximation for different cells compared with the TV of the exact solution. The TV of the approximate solutions have the same behavior as the TV of the exact solution. The value of the TV of the approximate solutions never

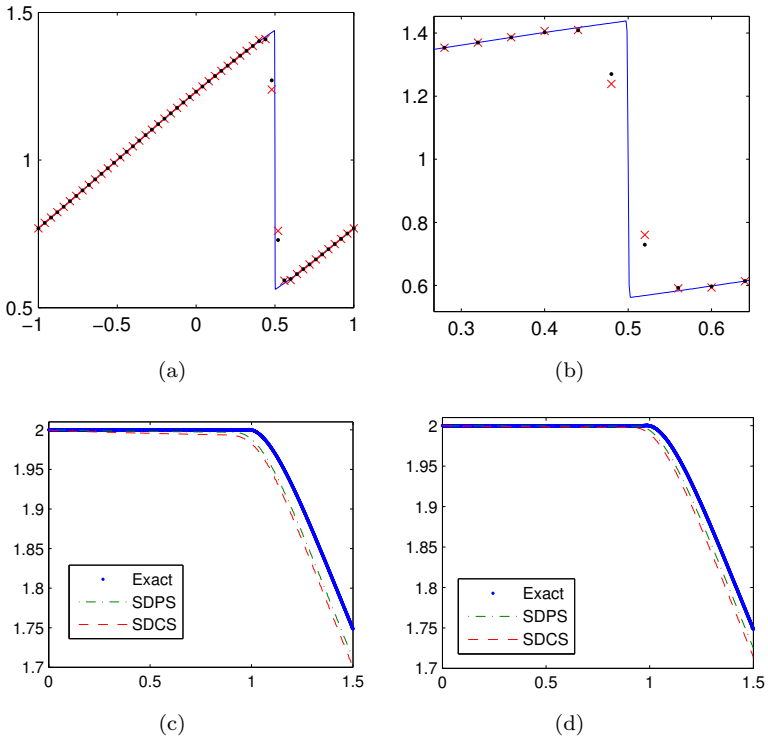

Figure 3. Problem 3 with $N = 50$. (a): the solution after shock formation at T=1.5. (b): zoomed region. (c) and (d): the change in the TV of the approximation for different cells(left $N = 100$ and right $N = 200$). SDPS, SDCS and exact solution are shown by " $\times$ ", " $\cdot$ " and solid line respectively.

increase above the exact TV. Both numerical results converge to the exact one, but it can be seen that the computed TV from SDPS are nearer to the TV of the exact solution. The TV of the approximate solutions are different from that of the exact solution for two reasons: (a): the TV is computed on a discrete set of points, (b): the discrete values of the numerical solution are not exact.

3.2 *Systems of Conservation Laws*

In this subsection the new semi-discrete schemes are used to solve hyperbolic systems of conservation laws. In particular, we solve the Euler equations of gas dynamics for a polytropic gas:

$$\frac{\partial}{\partial t}\begin{pmatrix}\rho\\ \rho q\\ E\end{pmatrix}+\frac{\partial}{\partial x}\begin{pmatrix}\rho q\\ \rho q^2+p\\ q(E+p)\end{pmatrix}=0,$$

$$p=(\gamma-1)(E-\frac{1}{2}\rho q^2),\qquad \gamma=1.4. \quad (14)$$

The time step dynamically with CFL restriction

$$\Delta t=\frac{0.9\lambda_{\max}h}{\max_j(c_j+|q_j|)},$$

are choosed. c_j and q_j are the local sound speed and velocity, respectively. This time step evaluation technique can accommodate for problems where the characteristic speeds change wildly in time.

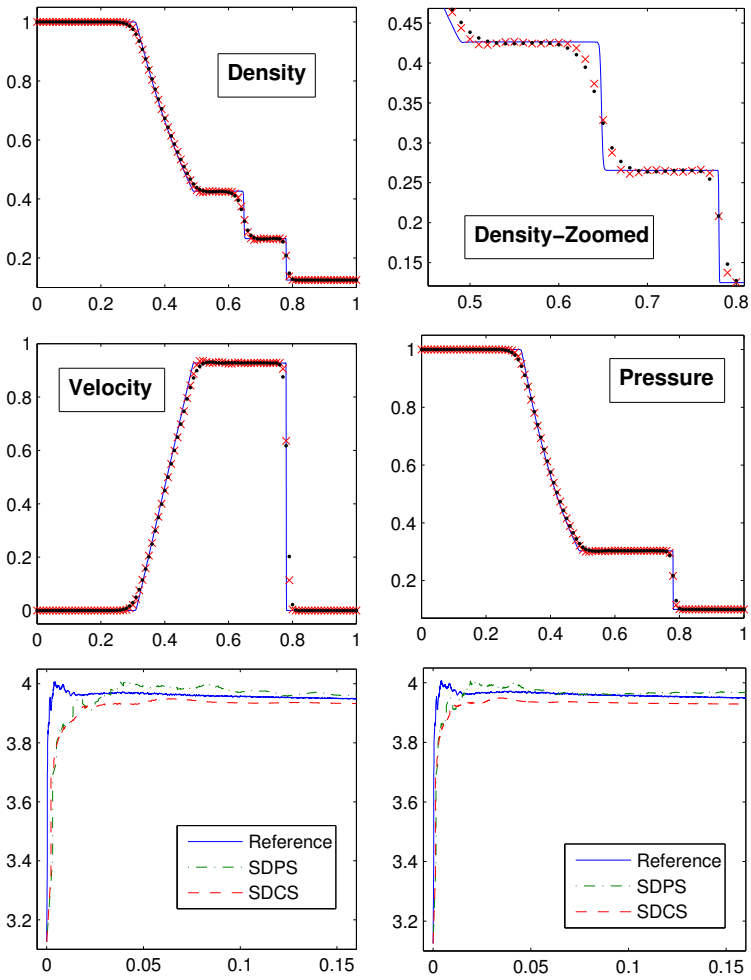

Figure 4. Top and center: Sod problem with $N = 100$. Bottom: the change in the TV of the approximation for different cells(left $N = 200$ and right $N = 400$) compared with the TV of a reference solution. SDPS, SDCS and reference solution are shown by " $\times$ ", " $\cdot$ " and solid line respectively.

First, the sod problem proposed in [26] is solved on the domain $[0, 1]$ with initial data:

$$u(x,0) = \begin{cases} (1,0,2.5)^T & 0 \leqslant x < 0.5, \\ (0.125,0,0.25)^T & 0.5 \leqslant x \leqslant 1. \end{cases}$$

Fig.4 shows the performance of the semi-discrete schemes at $T = 0.16$ with $N = 100$. We observe that the shock and the contact discontinuity are well-captured at low resolution. The SDPS scheme is sharper and less oscillatory than the SDCS scheme in particular for the density profile of this Riemann problem. Also, Fig.4 shows the TV behavior of the approximation, compared with a reference solution. The SDPS scheme overestimates the TV more than the SDCS schme as the problem is advanced in time, but converges to the TV of the reference solution over time. Next, the new semi-discrete schemes to the Lax problem are applied. In this test which is taken from[14] Eq. (14) is solved with the initial condition:

$$u(x,0) = \begin{cases} (0.445, 0.31061, 8.92840289)^T & 0 \leqslant x < 0.5, \\ (0.5,0,1.4275)^T & 0.5 \leqslant x \leqslant 1, \end{cases} \quad x \in [0,1].$$

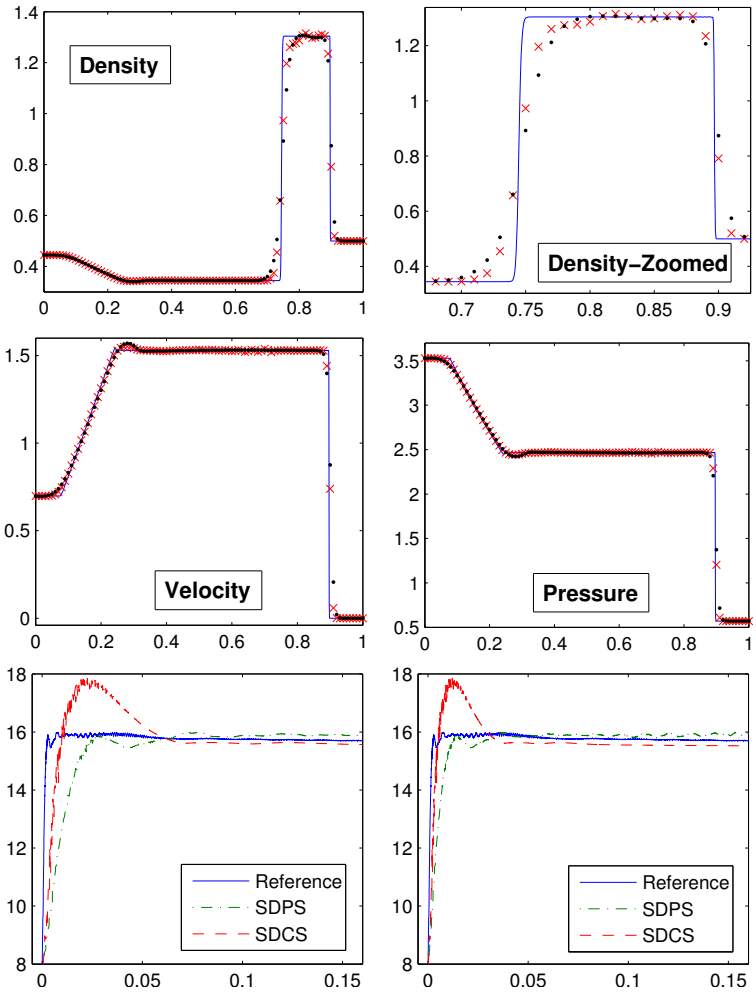

Figure 5. Top and center: Lax problem with $N = 100$. Bottom: the change in the TV of the approximation for different cells(left $N = 200$ and right $N = 400$) compared with the TV of a reference solution. SDPS, SDCS and reference solution are shown by " $\times$ ", " $\cdot$ " and solid line respectively.

For this more difficult shock tube problem, Fig. 5 shows the performance of the new schemes with $N = 100$ at $T = 0.16$. Similar to the Sod's test problem, the shock and the contact discontinuity are well-captured at low resolution, and SDPS is sharper and less oscillatory than SDCS. Also, Fig.5 shows the TV at $T = 0.16$ for different number of cells with SDPS and SDCS. We see that the TV of SDPS scheme is initially greater than that of the reference solution, but similar to the Sod problem, converges to the TV of the reference solution over time. The computed TV from SDPS is nearer to the TV of the reference solution. For $N = 200$ and 400, SDCS scheme gives a TV bounded by a maximum in the form of a peak reached after the first few steps and is then damped. The maximum bound is obtained earlier in time as the grid is refined, and then the TV comes close to the reference one. It is interesting, however, that the over-shoot of the TV at early times does not seem to depend on the mesh resolution.

For next example(known as Woodward and Colella Bang test) which is taken from[27], the Euler equations (14) is solved with a shock interaction problem. The solid wall boundary conditions are applied to both ends and the initial data on the

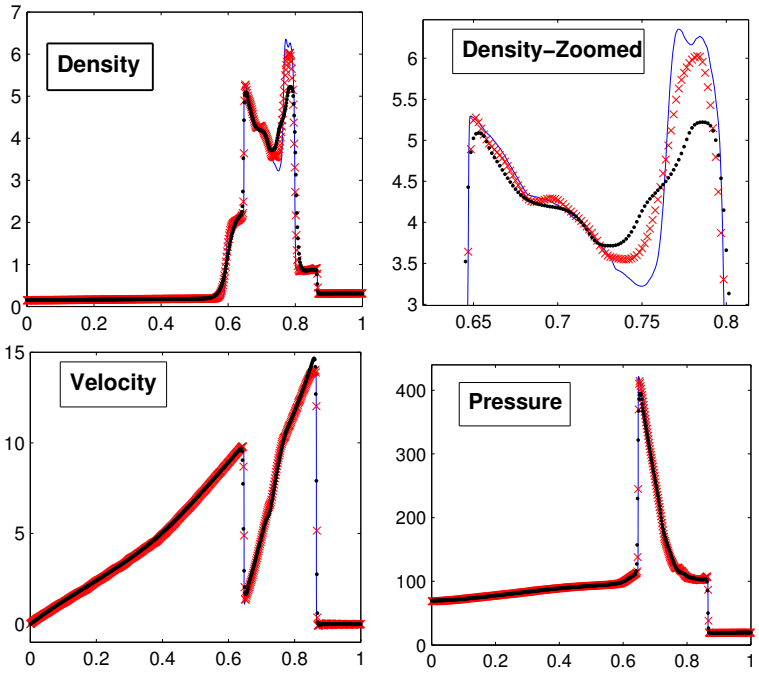

Figure 6. Results for the Woodward-Colella problem with $N = 800$ at $T = 0.038$. SDPS, SDCS and reference solution are shown by " $\times$ ", " . " and solid line respectively.

domain $x \in [0, 1]$ is:

$$u(x,0) = \begin{cases} (1,0,2500)^T & 0 \leqslant x < 0.1, \\ (1,0,0.025)^T & 0.1 \leqslant x < 0.9, \\ (1,0,250)^T & 0.9 \leqslant x \leqslant 1. \end{cases}$$

The numerical results of the density, velocity and pressure profile of this complex problem are shown in Fig.6. The results are with $N = 800$ at $T = 0.038$, and a reference solution is obtained using 4000 cells. some numerical oscillations are observed. the SDPS scheme captures the shocks interaction, and in the zoomed region we see that SDPS is sharper and behaves better with respect to oscillations compared to the SDCS scheme on 800 cells. The TV of the numerical solutions(not shown here) converges to the TV of the reference solution, but does not seem to converge over time. This is not surprising since this example contains sharp peaks that will not be resolved for coarse meshes.

For the final test(known as shock-Entrop test) which is taken from[24] the Euler equations (14) is solved with a moving Mach = 3 shock interacting with sine waves in density i.e.,

$$u(x,0) = \begin{cases} (3.85714, 10.1418096304, 39.16655928489427)^T & -5 \leqslant x < -4, \\ (1 + 0.2\sin(5x), 0, 2.5)^T & -4 \leqslant x \leqslant 5. \end{cases}$$

The flow contains physical oscillations which have to be resolved by the numerical methods. The solution is computed at $T = 1.8$. The numerical approximations of the density profile obtained by SDPS and SDCS are shown in Fig.7 along with a reference solution computed with 5000 cells. In the zoomed region, it can be observed the SDPS scheme is sharper than the SDCS scheme. Fig.7 also displays the TV behavior of the approximation, compared with the reference solution. It can be observed that the TV of our approximations converges to that of the reference

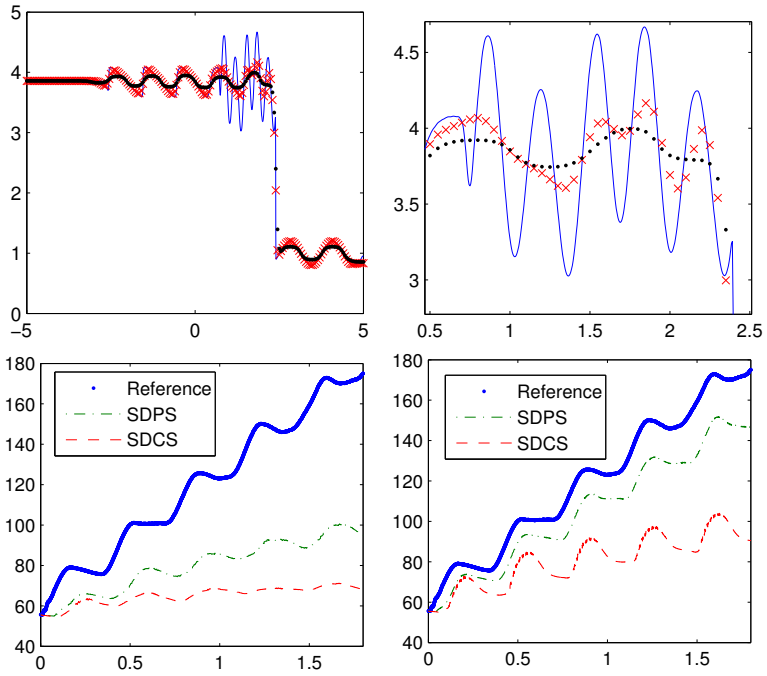

Figure 7. Top: results for the Shock-Entrop test with $N = 200$ at $T = 1.8$. Bottom: the change in the TV of the approximation for different cells(left $N = 200$ and right $N = 400$) compared with the TV of a reference solution. SDPS, SDCS and reference solution are shown by " $\times$ ", " $\cdot$ " and solid line respectively.

solution, but it can be seen that the computed TV from SDPS are nearer to the TV of the reference solution.

4. Conclusion

In this work, we have introduced two high-order, semi-discrete, central-upwind schemes for computing approximate solutions of 1D systems of conservation laws. First, we would like to comment that these schemes can be easily generalized to 2D problems (dimension-by-dimension finite volume approach). Numerical experiments on scalar problems show that the new schemes resolve discontinuities sharply while maintaining a non-oscillatory profile. In comparison to the SDCS, it can be seen that SDPS is sharper and behaves better with respect to oscillations. Also, the behavior of the total variation (TV) of the approximate solution obtained with these schemes is checked and observed that the TV of numerical solution is bounded for the test cases considered. In particular these schemes are applied to solve Euler equations of gas dynamics. We observed that the TV approaches the TV of the reference solution in various ways for various cases. For example, in the Shock-Entrop problem it is monotone while, in the Woodward-Colella problem it is not.

References

[1] S. Bryson and D. Levy, *On the Total Variation of High-Order Semi-Discrete Central Schemes for Conservation Laws*, J. Sci. Comput, **27** (2006) 163-175.
[2] S. Bryson and D. Levy, *High-order semi-discrete central-upwind schemes for multi-dimensional Hamilton-Jacobi equations*, J. Comput. Phys, **189** (2003) 63-87.
[3] F. Bianco, G. Puppo and G. Russo, *High-order central schemes for hyperbolic systems of conservation laws*, SIAM J. Sci. Comput, **21** (1999) 294-322.

[4] K. O. Friedrichs and P. D. Lax, *Systems of conservation equations with a convex extension*, Proc. Nat. Acad. Sci, **68** (1971) 1686-1688.
[5] E. Gabetta, L. Pareschi and M. Ronconi, *Central schemes for hydrodynamical limits of discrete-velocity kinetic models*, Trans. Theo. Stat. Phys, **29** (2000) 465-477.
[6] S. K. Godunov, *A finite difference method for the numerical computation of discontinuous solutions of the equations of fluid dynamics*, Math. Sb, **47** (1959) 271-290.
[7] A. Harten, B. Engquist, S. Osher and S. Chakravarthy, *Uniformly high order accurate essentially non-oscillatory schemes III*, J. Comput. Phys, **71** (1987) 231-303.
[8] A. Harten and S. Osher, *Uniformly high-order accurate nonoscillatory schemes, I*, SIAM J. Numer. Anal, **24** (1987) 279-309.
[9] G. S. Jiang and C. W. Shu, *Efficient implementation of weighted ENO schemes*, J. Comp. Phys, **126** (1996) 202-228.
[10] A. Kurganov and D. Levy, *A third-order semi-discrete central scheme for conservation laws and convection-diffusion equations*, SIAM J. Sci. Comput, **22** (2000) 1461-1488.
[11] A. Kurganov, S. Noelle and G. Petrova, *Semi-discrete central-upwind schemes for hyperbolic conservation laws and Hamilton-Jacobi equations.*, SIAM J. Sci. Comput, **23** (2001) 707-740.
[12] A. Kurganov and G. Petrova, *A third-order semidiscrete genuinely multidimensional central scheme for hyperbolic conservation laws and related problems*, Numer. Math, **88** (2001) 683-729.
[13] A. Kurganov and E. Tadmor, *New high-resolution central schemes for non-linear conservation laws and convection-diffusion equations*, J. Comput. Phys, **160** (2000) 241-282.
[14] P. D. Lax, *Weak solutions of non-linear hyperbolic equations and their numerical computation*, Comm. Pure Appl. Math, **7** (1954) 159-193.
[15] R. J. LeVeque, *Numerical Methods for Conservation Laws*, Lectures in Mathematics, Birkhuser, Basel, (1992).
[16] D. Levy, G. Puppo and G. Russo, *Central WENO schemes for hyperbolic systems of conservation laws*, Math. Model. Numer. Anal, **33** (1999) 547-571.
[17] D. Levy, G. Puppo and G. Russo, *On the behavior of the total variation in CWENO methods for conservation laws*, Appl. Numer. Math, **33** (2000) 407-414.
[18] D. Levy, G. Puppo and G. Russo, *Compact central WENO schemes for multidimensional conservation laws*, SIAM J. Sci. Comput, **22** (2000) 656-672.
[19] X. D. Liu, S. Osher and T. Chan, *Weighted essentially non-oscillatory schemes*, J. Comput. Phys, **115** (1994) 200-212.
[20] H. Nessyahu and E. Tadmor, *Non-oscillatory central differencing for hyperbolic conservation laws*, J. Comput. Phys, **87** (1990) 408-463.
[21] A. A. I. Peer, A. Gopaul, M. Z. Dauhoo and M. Bhuruth, *A new fourth-order non-oscillatory central scheme for hyperbolic conservation laws*, Appl. Numer. Math, **58** (2008) 674-688.
[22] A. A. I. Peer, A. Gopaul, M. Z. Dauhoo and M. Bhuruth, *New high-order ENO reconstruction for hyperbolic conservation laws*, Proceedings of the 2005 Conference on Computational and Mathematical Methods on Science and Engineering, (2005) 446-455.
[23] G. Russo, *Central schemes for conservation laws with application to shallow water equations*, in Trends and applications of mathematics to mechanics: STAMM 2002, Springer-Verlag, Italia SRL, (2005) 225–246.
[24] C. W. Shu and S. Osher, *Efficient implementation of essentially non-oscillatory shock-capturing schemes*, J. Comput. Phys, **77** (1988) 439-471.
[25] M. Simpson and K. Landman, *Nonmonotone chemotactic invasion: high-resolution simulation, phase plane analysis and new benchmark problems*, J. Comput. Phys, **225** (2007) 6-12.
[26] G. Sod, *A survey of several finite difference metods for systems of non-linear hyperbolic conservation laws*, J. Comput. Phys, **27** (1978) 1-31.
[27] P. Woodward and P.Colella, *The numerical solution of two-dimensional fluid flow with strong shocks*, J. Comput. Phys, **54** (1984) 115-173.